nature communications

Article

https://doi.org/10.1038/s41467-024-51755-2

The significance of electrical signals in maturing spermatozoa for phosphoinositide regulation through voltage-sensing phosphatase

Received: 29 April 2024

Accepted: 14 August 2024

Published online: 24 August 2024

Check for updates

Takafumi Kawai[1] ✉, Shin Morioka[2], Haruhiko Miyata[3], Rizki Tsari Andriani[1], Sharmin Akter[1,9], Gabriel Toma[4,10], Tatsuya Nakagawa[3,5], Yuki Oyama[3,5], Rie Iida-Norita[3], Junko Sasaki[2], Masahiko Watanabe[6], Kenji Sakimura[7], Masahito Ikawa[3,5], Takehiko Sasaki[2] & Yasushi Okamura[1,8]

Voltage-sensing phosphatase (VSP) exhibits voltage-dependent phosphatase activity toward phosphoinositides. VSP generates a specialized phosphoinositide environment in mammalian sperm flagellum. However, the voltage-sensing mechanism of VSP in spermatozoa is not yet characterized. Here, we found that VSP is activated during sperm maturation, indicating that electric signals in immature spermatozoa are essential. Using a heterologous expression system, we show the voltage-sensing property of mouse VSP (mVSP). The voltage-sensing threshold of mVSP is approximately −30 mV, which is sensitive enough to activate mVSP in immature spermatozoa. We also report several knock-in mice in which we manipulate the voltage-sensitivity or electrochemical coupling of mVSP. Notably, the V312R mutant, with a minor voltage-sensitivity change, exhibits abnormal sperm motility after, but not before, capacitation. Additionally, the V312R mutant shows a significant change in the acyl-chain profile of phosphoinositide. Our findings suggest that electrical signals during sperm maturation are crucial for establishing the optimal phosphoinositide environment in spermatozoa.

The membrane potentials of plasma membranes act as critical "electrical signals", enabling neurons and other cells to communicate and transmit information. Therefore, the physiological implications of these signals have predominantly been explored in neurons or muscles, with a primary focus on voltage-gated ion channels that modulate ion permeability based on membrane potential[1]. In contrast, our previous work identified a distinctive voltage-sensing phosphatase (VSP) which shows the voltage-dependent phosphatase activity toward phosphoinositides (PIPs). This property is due to the unique architecture of VSP which has a voltage-sensor domain (VSD), phosphatase domain (PD) and VSD-PD linker[2,3]. VSD, which is also conserved in the conventional voltage-gated ion channels, consists of four transmembrane helical segments (S1-S4) and the S4 segment contains positive charge residues for sensing the membrane potentials. PD shows

[1]Graduate School of Medicine, Osaka University, Suita, Japan. [2]Department of Biochemical Pathophysiology/Lipid Biology, Medical Research Institute, Tokyo Medical and Dental University, Tokyo, Japan. [3]Research Institute for Microbial Diseases, Osaka University, Suita, Japan. [4]Center for Medical Research and Education, Osaka University, Suita, Japan. [5]Graduate School of Pharmaceutical Sciences, Osaka University, Suita, Japan. [6]Faculty of Medicine, Hokkaido University, Sapporo, Japan. [7]Brain Research Institute, Niigata University, Niigata, Japan. [8]Graduate School of Frontier Bioscience, Osaka University, Suita, Japan. [9]Present address: Department of Physiology, Bangladesh Agricultural University, Mymensingh, Bangladesh. [10]Present address: Graduate School of Frontier Biosciences, Osaka University, Suita, Japan. ✉e-mail: kawai@phys2.med.osaka-u.ac.jp

https://doi.org/10.1038/s41467-024-51755-2

similarity to PTEN, which shows phosphatase activities toward PIPs. The VSD-PD linker connects PD with the VSD and plays crucial role in coupling VSD and PD activities. Thus, this unique configuration endows VSP with the capability to voltage-dependently dephosphorylate PIPs, thereby transforming "electrical signals" into "chemical signals"[3–7].

Recently, our study revealed the functional expression of VSP in mouse spermatozoa, elucidating its role in regulating sperm motility during capacitation through analysis of VSP-deficient animal models[8]. VSP induced notable alterations in the PIPs profile of mature spermatozoa, creating a distinctive longitudinal PI(4,5)P_2 (Phosphatidylinositol 4,5-bisphosphate) gradient along the flagella. This specialized PI(4,5)P_2 environment emerged as crucial for modulating the activity of SLO3, a sperm-specific K^+ channel pivotal for fertilization[8–10]. However, several fundamental questions persist regarding the functional role of VSP in spermatozoa: Does VSP really sense the membrane potential of spermatozoa? If this is the case, what is the mechanism underlying it?

The voltage-dependent enzymatic activity of VSP was initially characterized in *Ciona intestinalis* (Ci-VSP) using *Xenopus* oocyte heterologous expression systems[2]. This activity was subsequently identified in vertebrates, including zebrafish (Dr-VSP), African clawed frogs (Xl-VSP), and chickens (Gg-VSP) in vitro[11–14]. However, attempts to detect voltage-dependent phosphatase activities using mammalian VSPs in heterologous expression systems have been unsuccessful, despite their structural homologies with non-mammalian VSPs[3,15]. Consequently, the existence of voltage-sensing capabilities in mammalian VSPs remains uncertain, contributing to a dearth of detailed information regarding the electrophysiological properties of these proteins.

Here, we started our study by investigating the PIPs profile at different stages of sperm maturation. Our findings reveal a progressive impact of VSP on the PIPs profile during sperm maturation, suggestive of continuous VSP activation throughout this long-term process. Additionally, two-electrode voltage clamp (TEVC) analysis of mVSP activity, with modifications to its intracellular linker and N-terminal sequence in a heterologous expression system, indicated that mVSP is activated at approximately −30mV, a membrane potential lower than the resting membrane potential of immature spermatozoa.

Finally, we generated three distinct knock-in mice expressing VSP mutations: (1) loss of voltage-sensing capability (D225R), (2) loss of electrochemical coupling between voltage-sensor and enzyme (K347Q), and (3) slightly altered voltage-dependency (V312R), based on the aforementioned TEVC experiments. While functionally null D225R and K347Q mutant mice abolished VSP expression itself, V312R mutant mice exhibited normal protein expression with significant changes in spermatozoa function. This study provides pioneering insights into the significance of voltage-sensing capabilities of mVSPs in native spermatozoa.

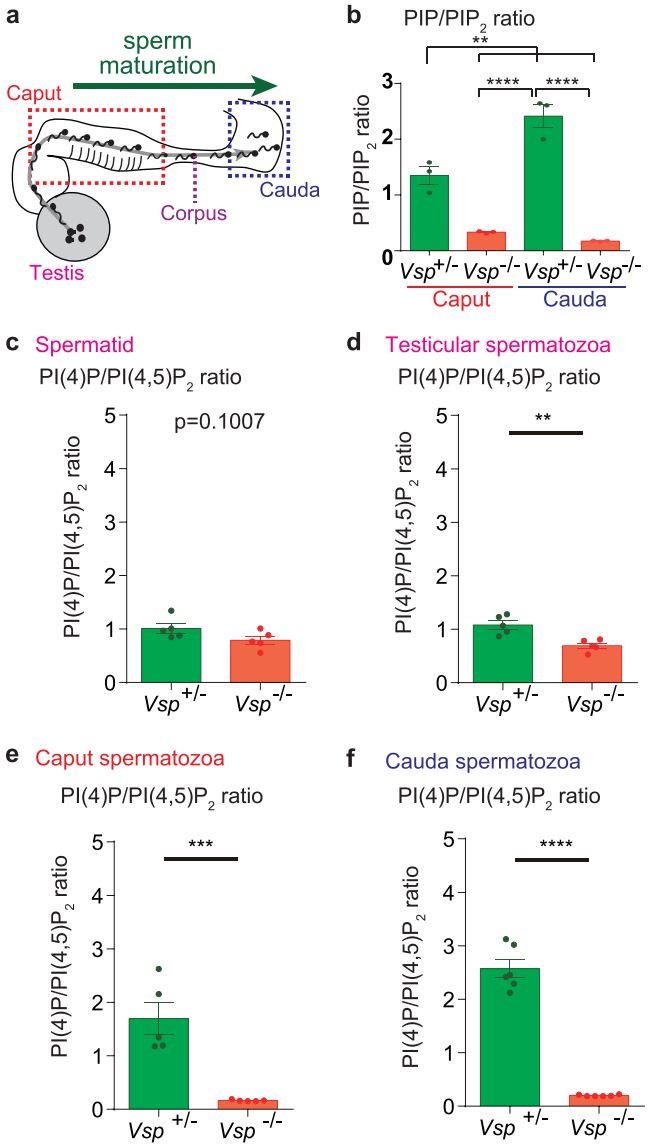

Fig. 1 | VSP shows the phosphatase activity in maturing spermatozoa. **a** Spermatozoa, which differentiate in the testis, undergo maturation as they are transported through the caput epididymis to the cauda epididymis. By the time they reach the cauda epididymis, they become fully mature and are capable of fertilization. The matured spermatozoa are stored in the epididymal cauda. **b** PIP/PIP_2 ratio in spermatozoa from caput and cauda epididymis of each genotype mice. The significant difference of PIP/PIP_2 ratio between $Vsp^{+/-}$ and $Vsp^{-/-}$ was already observed in caput epididymal spermatozoa, but the difference is more pronounced in cauda epididymal spermatozoa (Tukey's multiple comparison test. *p*-value is adjusted for multiple comparison. $^{**}p < 0.01$, $^{****}p < 0.0001$, $n = 3$ independent mice for each group). The exact *p*-value is shown in the Data Source file. Data are represented as mean ± s.e.m. **c**–**f** PRMC-MS analysis was performed at different maturation stages of spermatozoa. The calculated PI(4)P/PI(4,5)P_2 ratios are shown. (unpaired two-sided t-test, $^{**}p < 0.01$, $^{***}p < 0.01$, $^{****}p < 0.0001$). The data from cauda epididymis (**f**) was already reported in the previous study[8]. The experiment group in caput epididymis (**e**) corresponds to the experiment group of "low K^+" shown in Supplementary Fig. 4. For (**c**–**f**), $n = 5,5,5$ and 6 biologically independent mice in each genotype are used, respectively. Data are represented as mean ± s.e.m. The exact *p*-value is shown in the Data Source file.

Results

VSP demonstrates phosphatase activity during sperm maturation

Spermatozoa acquire fertility through a maturation process as they traverse from proximal to distal segments of epididymis, i.e., caput, corpus and cauda epididymis (Fig. 1a). This process is pivotal for optimal sperm function. Notably, the lipid composition of spermatozoa undergoes changes during this process[16]. While the membrane phospholipids contain acyl groups, with two fatty acids located at the sn-1 and sn-2 positions (Supplementary Fig. 1), it remains unknown how the profile of acyl chains of PIPs transitions during the maturation process. To elucidate it, we employed liquid chromatography-tandem mass spectrometry (LC-MS/MS) to assess the profiles of PIPs as well as phosphatidylserine (PS) in both caput and cauda epididymal spermatozoa. This method allows for the measurement of both the carbon number and the number of double bonds of the combined acyl groups at the sn-1 and sn-2 positions (Supplementary Fig. 1), while it does not separate the isomers of PIP (PI(3)P, PI(4)P, PI(5)P) and PIP_2 (PI(3,4)P_2, PI(3,5)P_2, PI(4,5)P_2) (Supplementary Fig. 1). In line with previous

findings[16], we observed a marked difference in PS composition between caput and cauda spermatozoa (Supplementary Fig. 2a). While PS contained only a limited set of acyl chain variants (Supplementary Fig. 2a), PIP and PIP_2 in both caput and cauda spermatozoa exhibited diverse acyl chain variants, particularly enriched in Long-Chain Polyunsaturated Fatty Acids (LC-PUFA) (e.g., 40:5 and 40:6) (Supplementary Fig. 2b, c). These LC-PUFA variants appear to include docosahexaenoic acid (DHA, 22:6) and docosapentaenoic acid (DPA, 22:5), which are highly prevalent in spermatozoa[17,18]. We confirmed the VSP protein expression at caput spermatozoa which is comparable to cauda spermatozoa (Supplementary Fig. 3). In cauda epididymis, the total PIP/PIP_2 ratio was significantly higher in mature sperm (cauda) than in immature sperm (caput) in $VSP^{+/-}$ samples (Fig. 1b). This trend was absent in VSP-deficient samples, suggesting that VSP exerts its phosphatase activity during the maturation process.

Subsequently, we investigated whether short-term alterations in membrane potential influence the PIPs profile using sperm from the caput epididymis. We manipulated the membrane potential of caput epididymal spermatozoa by incubating them in high or low extracellular K^+ solutions with 10 µM valinomycin for 30 minutes and employed Phosphoinositide Regioisomer Measurement by Chiral column chromatography and Mass Spectrometry (PRMC-MS), which can accurately separate PIPs regioisomers[8,19]. No significant difference in $PI(4)P/PI(4,5)P_2$ ratio was observed between the treatments (Supplementary Fig. 4), suggesting that a short-time electric signal is not sufficient and prolonged VSP activation is required for exhibiting the effect of phosphatase activity.

Then, we conducted PRMC-MS measurements using spermatids and testicular spermatozoa, which are at the earlier maturation stages (Fig. 1c, d and Supplementary Fig. 5 and 6, with cauda epididymis data included for comparison, as previously reported[8], in Fig. 1f). As shown in total $PI(4)P/PI(4,5)P_2$ ratio results (Fig. 1c–f), the differences in the ratios between $VSP^{+/-}$ and $VSP^{-/-}$ gradually increase over this long-term maturation period. Furthermore, while spermatids exhibited no difference in total $PI(4)P/PI(4,5)P_2$ ratio between the genotypes, a significant difference was noted in LC-PUFA-containing variants (40:5 and 40:6) (Supplementary Fig. 6a, *right*). Similarly, both in testicular spermatozoa and caput epididymal spermatozoa, a marked difference was evident for LC-PUFA-containing variants (e.g., 38:5, 38:6, 40:5, and 40:6) (Supplementary Fig. 6b, c, *right*), with these distinctions diminishing in cauda epididymis (Supplementary Fig. 6d, *right*). These results appear to suggest that mVSP may exhibit a preference for LC-PUFA during maturation, although the difference appears to be less obvious at the maturation stage, when the phosphatase activity is saturated.

mVSP activation occurs within the physiological voltage range of immature spermatozoa

Given that VSP demonstrates phosphatase activity during maturation, it is conceivable that the membrane potential of immature spermatozoa plays a crucial role in driving mVSP activity throughout its maturation process. We assessed the membrane potential of immature WT spermatozoa using the perforated patch clamp technique, preserving the intracellular environment. We observed that the averaged membrane potential of spermatozoa was -9.79 ± 1.23 mV ($n = 15$), consistently exceeding −30 mV in all recordings (Fig. 2a). Subsequently, we sought to determine if mVSP could be activated within this range of sperm membrane potential. Considering its structural resemblance to other VSPs (Fig. 2b), mVSP is anticipated to possess normal voltage sensitivity. However, as mentioned in the introduction, there are no successful reports demonstrating the voltage-dependent enzymatic activity of mammalian VSPs in vitro. This problem likely stemmed from the accumulation of mammalian VSPs in the Golgi apparatus of expression system cells, preventing their transportation to the plasma membrane[20]. Previous studies suggest that the N-terminal domains and intracellular loops of transmembrane proteins play crucial roles in trafficking to the plasma membrane[21–25]. Furthermore, while mVSP and Ci-VSP have an overall similar structure and conserved sequences, their sequences differ in the N-terminus and intracellular loops (Supplementary Fig. 7; full length: identity = 41.5%, similarity = 61.4%; N-terminus: identity = 18.9%, similarity = 40.0%). We addressed this by modifying mVSP, replacing the N-terminus and the intracellular S2-S3 loop with those of Ci-VSP, while preserving functionally critical regions: VSD, VSD-PD linker, and PD (Fig. 2c, d). This modification significantly enhanced the surface expression of mVSP in *Xenopus* oocytes (Fig. 2e, f). Here we refer to this molecule as mVSP*.

We then evaluated the voltage-dependent phosphatase activity of mVSP* using KCNQ2/3 channels as a readout for $PI(4,5)P_2$ levels (Fig. 2g, h). A notable decrease in KCNQ2/3 current occurred with prolonged depolarization-induced mVSP* activation, a phenomenon absents in non-modified original mVSP or enzyme-inactive mVSP* (mVSP* C458S), confirming its reliance on phosphatase activity. The voltage-dependency of mVSP* was further analyzed using GIRK (G protein-gated inwardly rectifying potassium channels) channels, applying repetitive 1-second voltage pulses with varying potentials (Fig. 2i). The threshold for mVSP* activation was approximately −30 mV, and the activity gradually increased up to +50 mV, which was the upper limit of the repetitive 1-second long-pulse protocol, due to contamination from endogenous currents. Notably, the change in GIRK current amplitude was not observed in C458S. These results unequivocally demonstrate that mVSP can be activated above −30mV, a range within the physiological membrane potential of immature spermatozoa.

Detailed analysis of the voltage dependency of mVSP and its mutants

Given the upper limitation of +50 mV for the analysis with GIRK channels, an alternative technique was employed to scrutinize the detailed voltage-dependent properties of mVSP. We utilized PLCδ1-PH-GFP, a well-established $PI(4,5)P_2$ probe (Fig. 3a), holding the membrane potential at −80 mV and applying a 10 s pulse protocol with different voltages up to +125 mV to examine the fluorescence change at the plasma membrane. Consistent with GIRK measurements, mVSP* activity was observed to begin around −30mV, reaching its maximum around +100 mV (Fig. 3b).

Subsequently, point mutation experiments were conducted (Fig. 3c), based on the reported mutations in other species of VSPs to elucidate the similarities and differences of mVSP with its counterparts. We initially examined the effect of mutation on VSD (Fig. 3c and d). The mutation on D225 in S1, considered a countercharge for Arg in S4 and essential for voltage-sensing capability[26], was examined. In alignment with previous studies[27,28], mVSP* D225R exhibited voltage insensitivity within the physiological range of membrane potential. Next, two distinct point mutations in S4, essential for the voltage sensing of voltage-sensor proteins, were induced: R309Q, generally demonstrating a large leftward shifted voltage dependency in diverse VSPs[11,14,29–33], and V312R, exhibiting a moderate leftward shift in VSD activity of Dr-VSP (T156R)[11]. Unexpectedly, R309Q did not impact the voltage sensitivity of mVSP*, contrary to previous reports on other VSPs. On the other hand, V312R moderately but significantly changed the voltage dependency of mVSP* leftward at a lower voltage (Fig. 3c, d), which is partly consistent with the observation in Dr-VSP[11]. These PLCδ1-PH-GFP results were corroborated in GIRK experiments (Supplementary Fig. 8), although differentiating between WT and V312R was challenging due to the limited information above +50 mV in GIRK recording. Additionally, a K347Q mutation in the VSD-PD linker region, critical for functional coupling[34], abolished voltage-dependent phosphatase activity (Fig. 3c–e). Furthermore, C458S, an enzyme dead mutant, displayed no VSP activity (Fig. 3c, f). We also confirmed that surface expression of mVSP* mutants remained unchanged (Fig. 3g–i).

https://doi.org/10.1038/s41467-024-51755-2

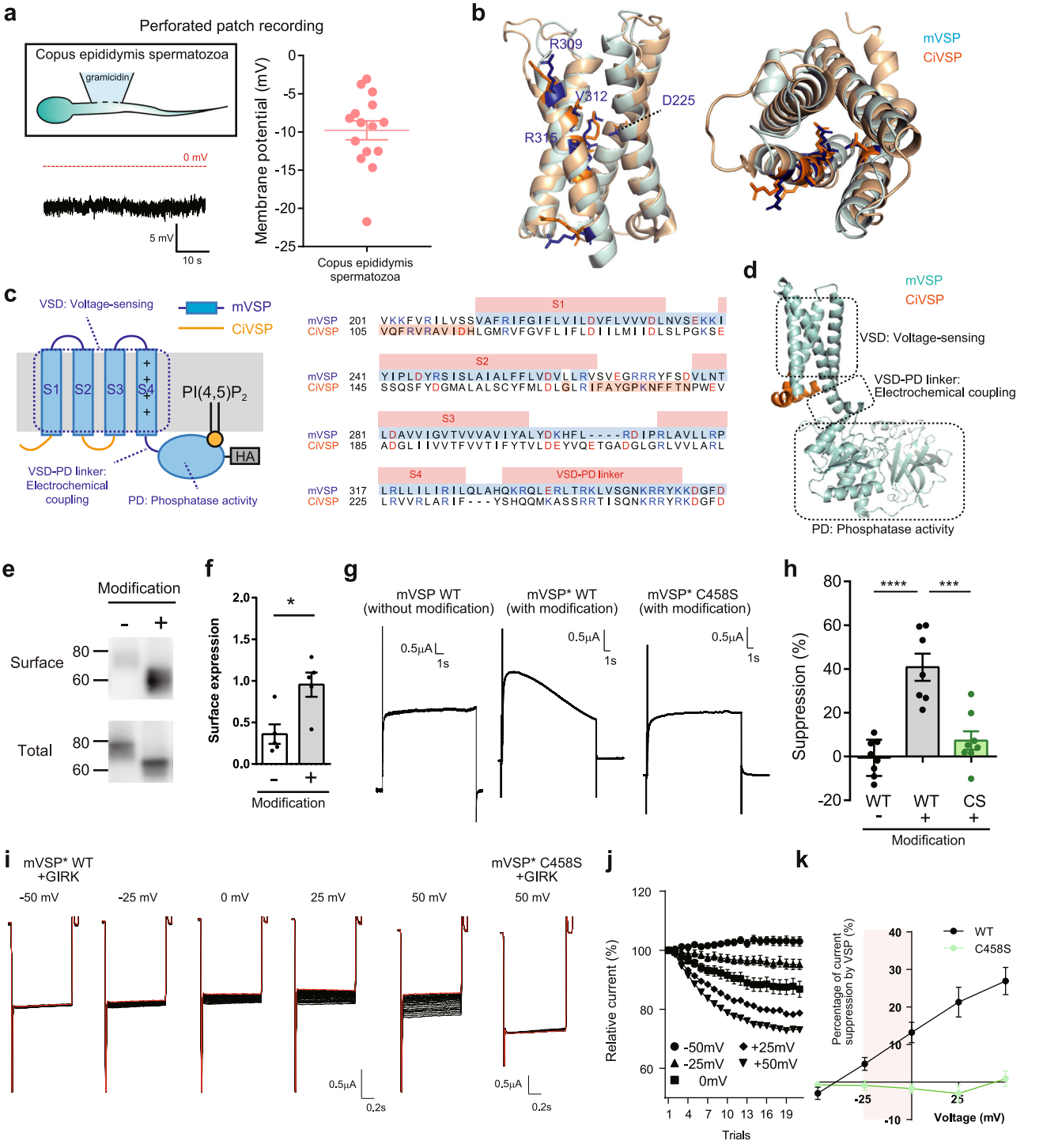

In summary, these findings suggest that the fundamental mechanisms of voltage sensing and electrochemical coupling in non-mammalian VSPs are largely conserved in mVSP, with subtle differences in the voltage-sensing machinery involving R309 of S4 when compared to other VSPs.

The mVSP V312R mutation affects sperm function

Our findings suggest that mVSP undergoes activation driven by the membrane potential of spermatozoa throughout the entire maturation process. To explore the voltage-sensing capability of endogenous mVSP in sperm flagellum, we generated three distinct knock-in mouse models featuring the V312R (moderately altered voltage sensitivity; Supplementary Fig. 9a), D225R (voltage-insensitive; Supplementary Fig. 9b), and K347Q (no VSD-PD coupling; Supplementary Fig. 9c) mutations, based on observations from in vitro experiments (Fig. 3). Functionally inert VSP mutants (D225R and K347Q) did not exhibit any VSP expression in spermatozoa (Fig. 4b), implying that a certain level of VSP activation is necessary for maintaining its expression in spermatozoa. Conversely, the quantity of endogenous VSP protein in spermatozoa of homogenous VSP V312R mice was comparable to that of wild-type VSP (Fig. 4b).

In a previous study, we found that VSP deficiency leads to abnormal sperm motility only after capacitation[8]. Therefore, we assessed the impact of the V312R mutation on sperm motility both before and after capacitation. We did not observe any differences in motility pattern between the wild-type and V312R homo spermatozoa

Fig. 2 | mVSP shows voltage-sensing phosphatase activity in the range of the resting membrane potentials of immature spermatozoa. a Recording of the resting membrane potential from immature spermatozoa. n = 15 cells examined over 7 independent mice. Data are represented as mean ± s.e.m. **b** The structural comparison of VSD between mVSP (light blue) and Ci-VSP (orange). The VSD structure of mVSP was predicted with ColabFold, an opensource software for protein structure prediction[54]. The VSD of Ci-VSP was solved in the previous study[26]. Some important residues are shown with the numbering of mVSP amino acids residues. **c** Schematic diagram of the modified mVSP (mVSP*). The voltage-sensing domain, linker region for electrochemical coupling, and phosphatase domain remained intact. The sequence alignment of the VSD between mVSP and Ci-VSP is also presented with amino acids from the experiment shaded in blue and orange, respectively. **d** The structure of the mVSP* was predicted with AlphaFold2. mVSP and Ci-VSP regions are shown in cyan and orange, respectively. The N terminus region is omitted. **e**, **f** Immunoblots against the surface proteins and total protein were detected by HA-antibody. The signals (**e**) and statistics (**f**) are shown. (*$p < 0.05$, unpaired two-sided t-test). $N = 5$ independent samples in (**f**). Data are represented as mean ± s.e.m. The exact p-value is shown in the Data Source file. **g** Voltage-dependent regulation of KCNQ2/3 activities by mVSP*. KCNQ2/3 was co-expressed with either the original mVSP, mVSP* WT or mVSP* C458S, an enzyme dead mutant. A +50 mV depolarization pulse was applied to activate both the VSPs and KCNQ2/3. The holding potential is −60mV. In mVSP* WT, the KCNQ2/3 current gradually decreased. In contrast, the current decrease was not observed in KCNQ2/3 co-expressed with either the mVSP or mVSP* C458S. **h** Statistical analysis for percent reduction of KCNQ2/3 currents. There was significant difference between WT and C458S (Tukey's multiple comparison test. p-value is adjusted for multiple comparison. ***$p < 0.001$, ****$p < 0.0001$). $N = 7$, 8 and 8 independent experiments for mVSP, mVSP* and mVSP* C458S, respectively. Data are represented as mean ± s.e.m. The exact p-value is shown in the Data Source file. Voltage-dependency of mVSP* was analyzed using GIRK current. **i** Representative traces and the time course of GIRK current amplitudes with repetitive mVSP* activation. 1 s depolarization pulses (to activate mVSP*) were applied 21 times in the intervals of test pulses (−120mV, 100 ms). The red trace indicates the 21st trace. **j** Time course of the percent current reduction across repeated pulses. $N = 11$ independent experiments. Data are represented as mean ± s.e.m. **k** The voltage-dependency of mVSP* was estimated from the percent current reduction at the 21st pulse in (**j**). $N = 11$ and 3 independent experiments for mVSP* and mVSP* C458S, respectively. Data are represented as mean ± s.e.m.

before capacitation (Fig. 4c). On the other hand, a substantial proportion of VSP V312R spermatozoa showed circular motion after capacitation which is significantly higher than wild-type littermates (Fig. 4d). We also analyzed velocity using different parameters in detail (Fig. 4e). Similarly, $Vsp^{VR/VR}$ spermatozoa exhibited a slight but significant difference in VCL (curvilinear velocity) and ALH (amplitude of lateral head) compared to $Vsp^{WT/WT}$ only after capacitation (Fig. 4g), but not before capacitation (Fig. 4f).

We also analyzed the PIPs profile in both immature and mature spermatozoa from the caput and cauda epididymis of $Vsp^{WT/WT}$ and $Vsp^{VR/VR}$ mice. Once again, the PI(4)P/PI(4,5)P_2 ratio progressively increased during sperm maturation in both $Vsp^{WT/WT}$ and $Vsp^{VR/VR}$ (Fig. 5a, b). The total PI(4)P/PI(4,5)P_2 ratio remained nearly identical between $Vsp^{WT/WT}$ and $Vsp^{VR/VR}$ in both the caput and cauda epididymis (Fig. 5b). However, LC-PUFA containing groups, especially 40:6, exhibited a trend of increase in $Vsp^{VR/VR}$ for both the caput and cauda epididymis (Fig. 5c–g). In summary, the VSP V312R mutation, characterized by a leftward shift in voltage sensitivity, appears to exert a moderate but significant effect on spermatozoa function, underscoring the importance of the membrane potential in VSP function.

Discussion

In this study, we have elucidated that VSP undergoes activation throughout sperm maturation, suggesting that the membrane potential of immature spermatozoa plays a crucial role in shaping the appropriate PIPs environment within the sperm flagellum (Fig. 6). This research marks the successful observation of the voltage-dependent enzymatic activity of mammalian VSPs in vitro, revealing that mVSP can be activated at the resting membrane potential of immature spermatozoa. Lastly, we discovered that the VSP mutant (V312R) with moderately shifted voltage-range-of-activation showed altered pattern of sperm motility and altered PIPs profile, further highlighting the importance of electric signal in maturing spermatozoa for VSP activation.

Spermatozoa undergo dynamic lipid remodeling during epididymal maturation[35]. Here, we report that the PIPs profile is altered during sperm maturation, with Long-Chain Polyunsaturated Fatty Acids (LC-PUFA) preferentially incorporated into PIPs as spermatozoa undergo maturation. Furthermore, we identify VSP as a key player in this process, indicating that VSP is partly responsible for the lipid remodeling in terms of PIPs composition.

Considering that the PIPs level is generally balanced between phosphoinositide phosphatase and kinase activities, it is crucial to evaluate the contribution of kinases to this process. A previous study investigated the expression of phosphatidylinositol 4-phosphate 5-kinase (PIP5K) in spermatogenesis[36]. They reported that the expression of PIP5K isozymes (PIP5K1A and PIP5K1B) is highest in elongated spermatids but significantly reduced in epididymal spermatozoa. Consistent with this finding, our study reveals a gradual decrease in the PI(4)P/PI(4,5)P_2 ratio from spermatids to immature spermatozoa in VSP-deficient spermatozoa. However, this ratio does not undergo substantial changes in spermatozoa from the caput to cauda epididymis (Fig. 1b). Overall, it is likely that PIP5K activity is relatively low in epididymal spermatozoa, with VSP emerging as the major regulator of PI(4,5)P_2 levels during epididymal maturation.

Notably, VSP exhibits a preference for targeting LC-PUFA during specific maturation stages (Supplementary Fig. 6). While the detailed molecular mechanism remains elusive, LC-PUFA, a newly incorporated lipid during maturation, maybe a susceptible target for VSP. Alternatively, our prior research unveiled that VSP establishes a heterogeneous distribution of PI(4,5)P_2 in the sperm flagellum[8], which raises the possibility that LC-PUFA may also display heterogeneous distribution in the sperm flagellum, facilitating easy access for VSP to these molecules.

In this study, we demonstrated the voltage-sensing phosphatase activity of mammalian VSP using a heterologous expression system. Previous studies only reported the functionality of the PD of mammalian VSP by generating chimeras in which the enzyme domain was replaced from Ci-VSP to mammalian VSPs[12,15,37]. However, VSP requires other several factors such as VSD motion and VSD-PD coupling, in addition to enzyme activity, for proper function[3]. Therefore, it had been crucial to confirm the activity with the entire mammalian VSP structure. The present modified mVSP (mVSP*), retaining the intact VSD, VSD-PD linker, and PD, exhibited normal voltage-sensing phosphatase activity, strongly supporting the role of mVSP as a voltage-sensing phosphatase.

In heterologous expression experiments, mVSP* displayed phosphatase activity above −30mV. This threshold is comparable to that reported for Ci-VSP[2,3] and even more negative than other VSPs such as those from zebrafish, chicken, and frogs[3,11–14]. Additionally, mVSP* showed conservation of the common activation machinery shared with other non-mammalian VSPs. For instance, the mutation of D225 residue in S1 which is supposed to form a salt-bridge with Arg in S4[3,26,38], completely abolished voltage-sensitivity consistent with the previous findings in Ci-VSD[27]. Furthermore, V312R mutation showed a moderate change in the voltage dependency, which is partially also consistent with the previous studies in Dr-VSP[11]. Similarly, the mutation K347Q in the VSD-PD linker of mVSP*, akin to other non-mammalian VSP[34], demonstrated a common coupling mechanism between VSD and PD. Unexpectedly, the R309Q mutation in mVSP*, corresponding

https://doi.org/10.1038/s41467-024-51755-2

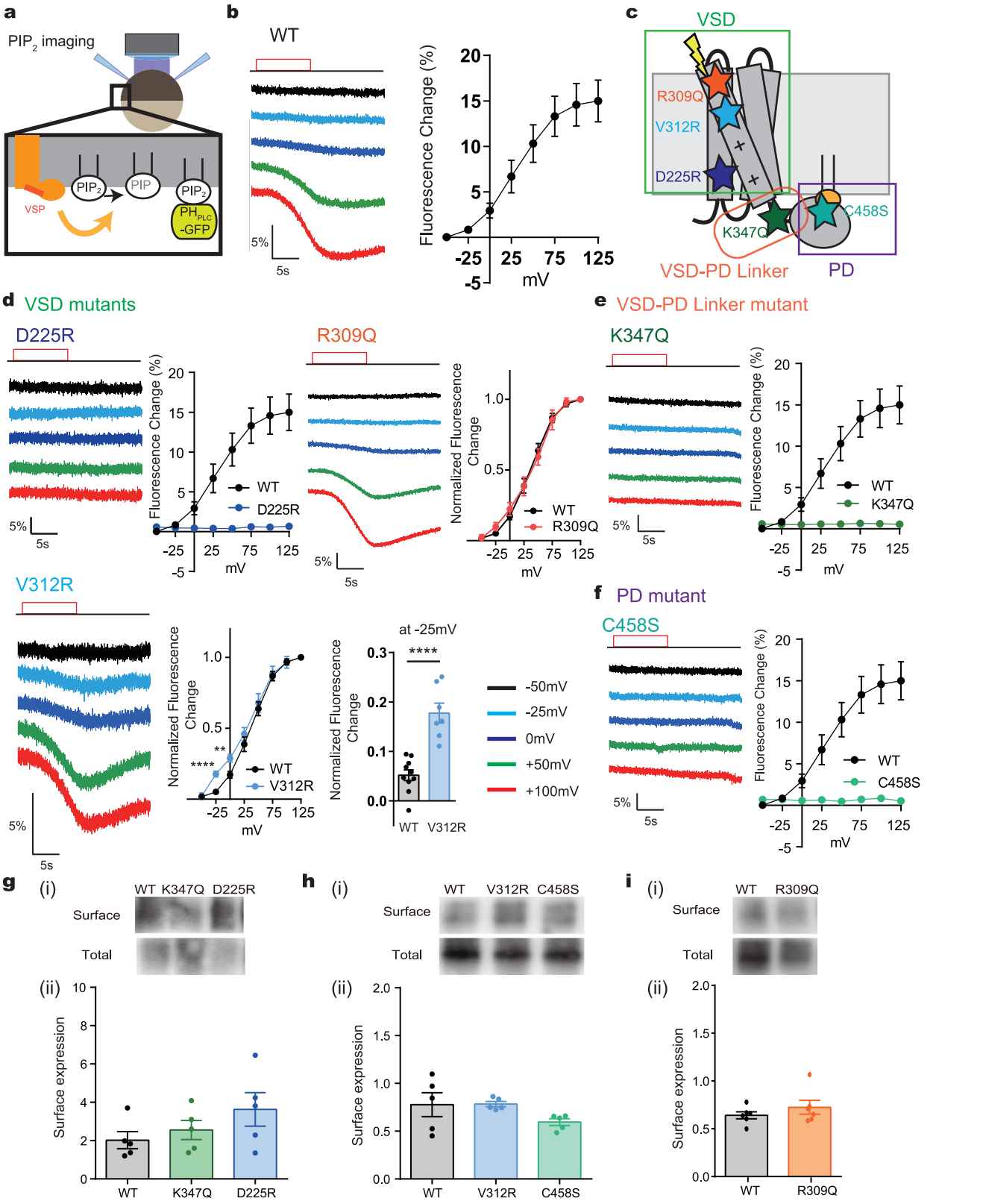

to R217Q in Ci-VSP, did not significantly alter voltage-sensitivity, contrary to previous reports for other VSPs[11,14,29–33]. This difference appears to suggest that the extracellular space of S4 in mVSP may have a distinct surface charge environment from other VSPs.

It is important to note that we modified the N-terminal and S2-S3 loop of mVSP for efficient expression in *Xenopus* oocytes. While this manipulation may potentially affect voltage-sensitivity, our previous study demonstrated that similar modifications of the N-terminal did not change the voltage-dependency of other VSPs or ion channels in *Xenopus* oocytes[21,22]. Also considering the lack of evidence that the intracellular S2-S3 loop critically regulates voltage-sensing phosphatase activity, despite comprehensive biophysical analyses of VSP[3], it is unlikely that modifications to the N-terminal or S2-S3 loop of mVSP confer voltage sensitivity.

Fig. 3 | Voltage-dependency analysis of mVSP mutants using PLCδ1PH-GFP combined with TEVC. a Schematic illustration of VCF experiments. **b** *Left*, Representative traces of fluorescence changes in mVSP*. 10 s pulses with different voltages were applied to observe fluorescence changes. The traces at various voltages are shown with different colors: black, cyan, blue, green, and red; to represent −50 mV, −25 mV, 0 mV, +50 mV and +100 mV, respectively. *Right*, The voltage-dependent activity of mVSP* WT as examined by fluorescence change. $N = 10$ independent experiments. Data are represented as mean ± s.e.m. **c** Schematic diagram showing the mutated residues targeted in the VCF experiment. Representative traces of fluorescence changes in mVSP* mutants. **d** Effect of mutations on VSD. D225R, R309Q and V312R were examined based on previous studies. $N = 5$, 6 and 7 independent experiments for D225R, R309Q and V312R, respectively. Because V312R showed significant difference from WT at −25 mV, it is also shown in the separate bar graph (Unpaired two-sided t-test, $^{****}p < 0.0001$). Data are represented as mean ± s.e.m. The exact *p*-value is shown in the Data Source file. **e** Effect of VSD-PD linker mutation. K347Q did not show any fluorescence change. $N = 5$. **f** Effect of PD mutation. C458S did not show any fluorescence change. $N = 4$ independent experiments. Data are represented as mean ± s.e.m. Surface protein expression of mVSP and its mutants (**g**, K347Q and D225R; **h**, V312R and C458S; **i**, R309Q) in *Xenopus* oocytes. Images (i) and statistics (ii) are shown. Unpaired two-sided t-test or Dunnett's multiple comparisons were performed for comparison with WT, but there was no significant difference. $N = 5$ independent samples in (**e**) and (**f**), while $n = 6$ independent samples in (**g**). Data are represented as mean ± s.e.m. The exact *p*-value with adjustment for multiple comparison is shown in the Data Source file.

Our study suggests that VSP undergoes activation during epididymal maturation, a crucial process for establishing proper PIPs environments in matured spermatozoa. Therefore, we aim to discuss the voltage-sensing mechanism of VSP during this maturation process. Our heterologous expression experiments indicate that VSP becomes activated above −30 mV, a membrane potential range observed in immature spermatozoa. It is important to consider the possibility that the less negative membrane potential of immature spermatozoa could be also due to an incomplete pipette seal during the recording. However, when performing voltage-clamp experiments on the same measurements, we observed clear voltage-dependent currents (Supplementary Fig. 11a), indicating that the quality of our measurements is reliable. Furthermore, alkalinizing the intracellular pH evoked a large hyperpolarization response in the same recording, which is consistent with previous papers (Supplementary Fig. 11b)[9]. Therefore, it appears that the influence of leakage on our measurements of membrane potential is limited.

Notably, the several studies report that ion composition of the mammalian epididymal lumen significantly differs from the experimental HEPES-based solutions[39–42]. For instance, the rat cauda epididymis is reported to contain approximately 55 mM K^+ and only 20 mM Na^+, potentially leading to a more depolarized state of spermatozoa compared to experimental conditions. Therefore, it is possible that extent of VSP activity in experimental condition was underestimated and VSP may be more efficiently activated at the resting membrane potential of epididymal spermatozoa.

Unexpectedly, single mutations in D225 (to R, causing voltage insensitivity) or K347 (to Q, resulting in no electrochemical coupling) eliminated VSP expression in spermatozoa (Fig. 4b), although these mutants showed normal surface expression in heterologous expression systems. This implies that the basal phosphatase activity is essential for maintaining VSP expression in spermatozoa, and it is also consistent with our previous finding that functionally inactive Venus-tagged VSP lacked protein expression itself in spermatozoa[8]. Building on this idea, the observation that voltage-insensitive mutants (D225R) do not exhibit VSP expression appears to suggest that voltage sensing is crucial for VSP activity in spermatozoa.

Besides, V312R, which has leftward shift of voltage range for activation, showed modifications in PIPs profiles as well as sperm motility in the present study. Notably, the V312R mutant showed a differential trend in the LC-PUFA-containing $PI(4,5)P_2$ variant, possibly related to the observation that VSP selectively targets LC-PUFA at certain maturation stages (Supplementary Fig. 6). In the motility analysis, V312R exhibited the phenotype only after capacitation. This result is important because the sperm motility was significantly changed only after capacitation in VSP-deficient spermatozoa in the previous study[8].

Previously, we observed that $PI(4,5)P_2$ levels are elevated in VSP-deficient spermatozoa, which enhances SLO3 activity and influences Ca^{2+} signaling during capacitation[8]. It is also possible that some other regulatory mechanism by $PI(4,5)P_2$ is important for the capacitation, because the V312R spermatozoa only showed the partial increase in $PI(4,5)P_2$ levels in some acyl groups. For example, our previous study demonstrated that $PI(4,5)P_2$ is heterogeneously distributed along the sperm flagella with some clusters[8], potentially affecting the localization of membrane proteins within the flagellum. Therefore, the altered $PI(4,5)P_2$ distribution might affect the protein localization that is important for capacitation. Interestingly, we observed that the expression of VSP itself is absent in mutants with severely impaired VSP function (D225R and K347Q). This result implies that the quantity of $PI(4,5)P_2$ potentially affect the expression of transmembrane proteins, including VSPs. It would be interesting, if VSP changes the expression profile of transmembrane proteins that are important for capacitation.

In conclusion, our results provide evidence for the critical role of voltage-sensing property of mVSP in spermatozoa. Future investigations into the regulatory mechanisms of membrane potential in maturing spermatids or spermatozoa will further enhance our understanding of the intricate relationship between membrane potential and enzyme activity.

Methods

Animals

In most experiments involving VSP-deficient animals, we utilized the same lineage as in our prior publication[8]. This lineage comprises VSP knock-in mice, where the PD was truncated at the active catalytic center, and Venus was fused at the end. Unexpectedly, this lineage lacked VSP protein in mature spermatozoa. Additionally, another VSP-deficient animal was generated to assess VSP protein expression in both immature and mature spermatozoa (See also Supplementary Fig. 3). All animal procedures were approved by the Animal Care and Use Committees of Osaka University.

Generation of another VSP-deficient mice

The pX330 plasmids expressing humanized Cas9 and single guide RNAs targeting exon 4 were injected into pronuclei of zygotes of B6D2F1 x B6D2F1 mice[43,44]. The sequence of gRNA is 5′-AGGTGTCAGTGAGTGCTTCA-3′. Embryos were cultured in KSOM overnight and subsequently transferred into the oviducts of pseudopregnant Institute of Cancer Research (ICR) outbred female mice. Screening of mutant pups was performed by direct sequencing following polymerase chain reaction (PCR) using primers (5′-ACCTGAAGCCATAGCTTAAGC-3′ and 5′-TTCTCCCACACTGGCTGGCTCAAG−3′). A founder mouse with an 1 bp insertion was used to expand the colony. The animal was backcrossed with C57BL/6 mice for three times. We confirmed that VSP protein expression is abolished in the homozygous mutant animals (Supplementary Fig. 3).

Plasmid and RNA Synthesis

mVSP was subcloned from mouse testis cDNA into the pSD64TF vector for cRNA synthesis. Hemagglutinin (HA)-tag sequence was introduced at the C-terminal of mVSP for detection in Western blotting. As

https://doi.org/10.1038/s41467-024-51755-2

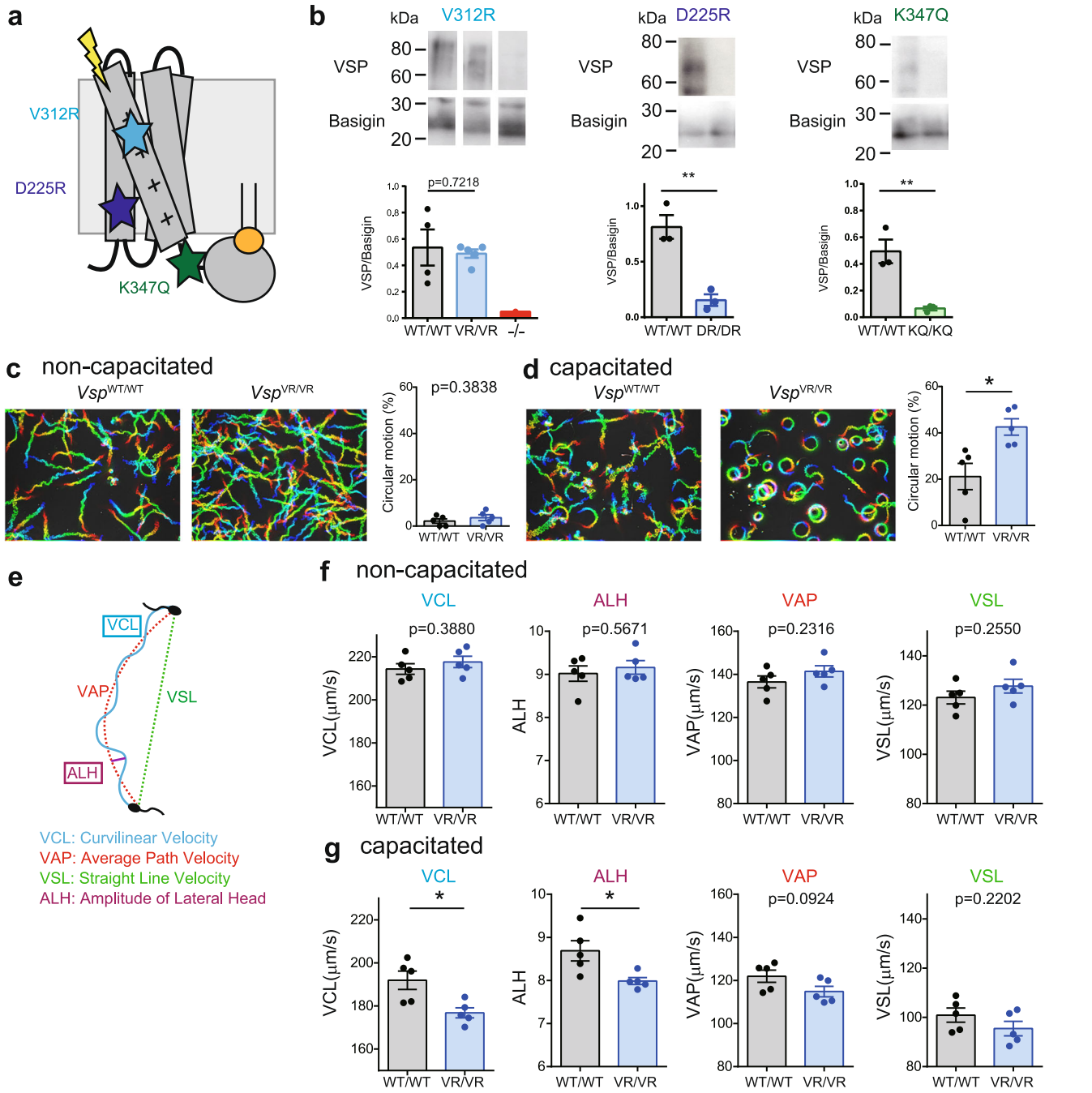

Fig. 4 | mVSP V312R shows moderate but significant change in sperm motility only after capacitation. a Schematic diagram shows the mutated residues targeted in the knock-in mouse experiment. **b** Western blotting results show the protein expression of mVSP and Basigin (positive control) in native spermatozoa of WT ($Vsp^{WT/WT}$), *Vsp* KO, V312R mutants ($Vsp^{VR/VR}$), D225R mutants ($Vsp^{DR/DR}$) and K347Q mutants ($Vsp^{KQ/KQ}$). In $Vsp^{DR/DR}$ and $Vsp^{KQ/KQ}$, the mVSP signal disappeared as well as *Vsp* KO. Unpaired two-sided t-tests were performed between the WT and homozygous mutants. $^{**}p < 0.01$. For V312R, $n = 4$, 5 and 1 independent mice for $Vsp^{WT/WT}$, V312R mutants ($Vsp^{VR/VR}$), and *Vsp* KO, respectively. For D225R, $n = 3$ independent mice for each genotype. For K347Q, $n = 3$ independent mice for each genotype. Data are represented as mean ± s.e.m. The exact *p*-value is shown in the Data Source file. **c**, **d** Analysis of sperm motility before (**c**) and after (**d**) capacitation in WT and $Vsp^{VR/VR}$. *Left*, Trajectories of spermatozoa isolated from WT and $Vsp^{VR/VR}$ mice. Spermatozoa were incubated for only 10 min in TYH (**c**), while 2 h in (**d**). *Right*, Statistical analysis was performed on the percentage of cells showing circular motion using unpaired two-sided *t*-test ($^{*}p < 0.05$). $N = 5$ independent mice for all experiment groups. Data are represented as mean ± s.e.m. The exact *p*-value is shown in the Data Source file. **e** Illustration of the parameters in sperm motility analysis. **f**, **g** Quantitation of sperm motility parameters of non-capacitated (**f**) and capacitated (**g**) spermatozoa. The individual parameters are described in (**e**). Unpaired two-sided *t*-test $^{*}p < 0.05$. $N = 5$ independent mice for all experiment groups. Data are represented as mean ± s.e.m. The exact *p*-value is shown in the Data Source file.

illustrated in Fig. 2, we replaced the N-terminal of mVSP (M1-S211) with that of Ci-VSP (M1-H115) and the S2-S3 loop of mVSP (V265-D276) with that of Ci-VSP (I169-N180) to design mVSP*. The nucleotide sequence of mVSP* is also shown in Supplementary Fig. 12 (see also Supplementary Table 1 for the primers). The number of amino acid residues in mVSP* (e.g., V312) is assigned with reference to the native mVSP. The GIRK2d (Kir3.2d) plasmid was provided by Dr. Yoshihisa Kurachi (Osaka University, Japan)[45]. G-protein β1 and γ1 subunit plasmids were provided by Dr. Toshihide Nukada (retired). KCNQ2/3 plasmids were provided by Dr. David McKinnon (Stony Brook University) and Dr.

https://doi.org/10.1038/s41467-024-51755-2

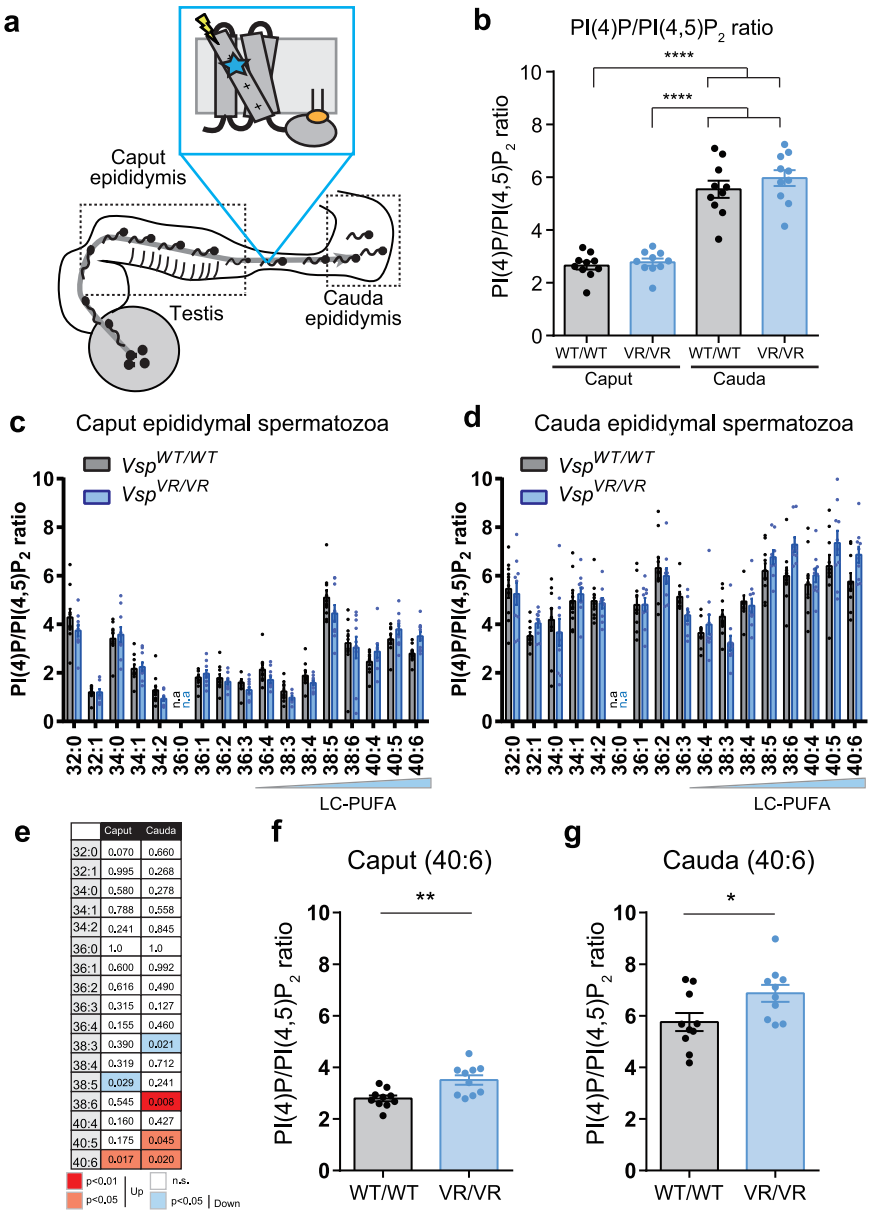

	Caput	Cauda
32:0	0.070	0.660
32:1	0.995	0.268
34:0	0.580	0.278
34:1	0.788	0.558
34:2	0.241	0.845
36:0	1.0	1.0
36:1	0.600	0.992
36:2	0.616	0.490
36:3	0.315	0.127
36:4	0.155	0.460
38:3	0.390	0.021
38:4	0.319	0.712
38:5	0.029	0.241
38:6	0.545	0.008
40:4	0.160	0.427
40:5	0.175	0.045
40:6	0.017	0.020

p<0.01 | Up | n.s.
p<0.05 | p<0.05 | Down

Fig. 5 | Spermatozoa of mVSP V312R show moderate phenotype in PI(4)P/PI(4,5)P_2 ratio especially in LC-PUFA containing acyl chains. a Schematic diagram showing the V312R mutation residue and different maturation stages of spermatozoa. **b** Total PI(4)P/PI(4,5)P_2 analysis of spermatozoa in caput and cauda epididymis from WT ($Vsp^{WT/WT}$) and V312R mutants ($Vsp^{VR/VR}$). There was no difference between the two genotypes, although the PI(4)P/PI(4,5)P_2 ratio significantly increased during maturation in both genotypes. (Tukey's multiple comparison test. *p*-value is adjusted for multiple comparison. ****$p < 0.0001$, $n = 10$ for each group). $N = 10$ independent mice for each genotype. Data are represented as mean ± s.e.m. The exact *p*-value is shown in the Data Source file. **c**, **d** PI(4)P/PI(4,5)P_2 ratio profiles are identified based on sn-1 and sn-2 acyl chains in $Vsp^{WT/WT}$ and $Vsp^{VR/VR}$ spermatozoa from caput (**c**) and cauda (**d**) epididymis. n.a. indicates that the calculation cannot be performed due to no PI(4,5)P_2 detection. $N = 10$ independent mice for each genotype, but the outlier is removed as appropriate. See also Source Data file. Data are represented as mean ± s.e.m. **e** Two-sided multiple-t test with no adjustments for multiple comparisons is performed and the *p*-value is shown in the table. The increases or decreases in $Vsp^{VR/VR}$ with a *p*-value < 0.05 were highlighted in red and blue, respectively. **f**, **g** The comparison of for (40:6) acyl chain in caput and cauda epididymis. (two-sided t-test., *$p < 0.05$ and **$p < 0.01$, respectively. $N = 10$ independent mice for each genotype. Data are represented as mean ± s.e.m. The exact *p*-value is shown in the Data Source file.

Koichi Nakajo (Jichi Medical University, Japan). Mutagenesis was performed using Primestar Max (Takara, Japan; see also Supplementary Table 1 for the primers). cRNA was synthesized using the mMESSAGE mMACHINE transcription kit (Thermo Fisher Scientific) after linearization with restriction enzymes.

Recordings of membrane potentials from immature spermatozoa

We performed perforated patch clamp recordings from immature spermatozoa to measure membrane potentials[8,46]. Sperm were isolated from the corpus epididymis in an HS-based solution containing (in mM): 135 NaCl, 5 KCl, 2 $CaCl_2$, 1 $MgSO_4$, 20 HEPES, 5 glucose, 10 lactic acid and 1 sodium pyruvate (pH 7.4). After 10 min, the supernatant was centrifuged, washed twice, resuspended in the HS-based solution, and placed on untreated glass coverslips. After 10 min, the coverslips were transferred to the recording chamber which was perfused with the HS-based solution. Recording pipettes were made of borosilicate glass (BF-150-86-10; Sutter Instruments, CA, USA) using a puller (P-97; Sutter Instruments). The intracellular solution contained (mM): 120 KCl, 3 $MgCl_2$, 40 HEPES, 0.3 EGTA (pH 7.0), and 0.05 mg/ml

https://doi.org/10.1038/s41467-024-51755-2

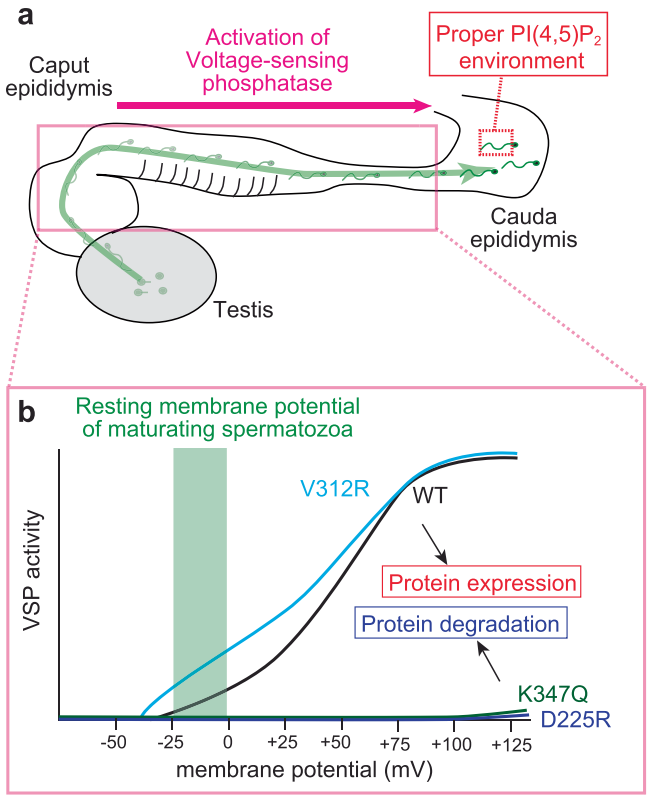

Fig. 6 | Schematic illustration showing the model for mVSP activation in spermatozoa. a mVSP activation during sperm maturation. Proper $PI(4,5)P_2$ environment of sperm flagellum, which is important for sperm function, is gradually formed during this process. **b** Voltage-dependency of mVSP in spermatozoa. We hypothesize that both V312R and WT are activated with resting membrane potential of maturing spermatozoa. D225R and K347Q shows protein degradation, because the basal phosphatase activity is required for VSP expression in spermatozoa.

gramicidin. We applied the negative pressure from the pipette to the cytoplasmic droplet of the spermatozoa to form the tight giga-ohm seal. After the giga-ohm seal, we waited for the pore formation by antibiotics which could be monitored by the access resistance. After pore formation, the access resistance was 50–100 MΩ. Recordings were performed using an Axopatch 200B (Molecular Devices, CA, USA) and sampled at 5 kHz using Digidata 1550 A (Molecular Devices) and pCLAMP 10.5 software (Molecular Devices).

Two-electrode voltage clamp recordings in oocytes

Xenopus oocytes were harvested from animals anesthetized in water containing 0.2% ethyl 3-aminobenzoate methanesulfonate salt (Sigma-Aldrich, St. Louis, MO). The oocytes were defolliculated by treating with type I collagenase (1.0 mg/mL; Sigma-Aldrich) in ND96 solution containing (in mM): 96 NaCl, 2 KCl, 5 HEPES, 1.8 $CaCl_2$, and 1 $MgCl_2$ (pH 7.5). The defolliculated oocytes were then injected with cRNA. Current recordings were conducted two days after cRNA injection by two-electrode voltage clamp (TEVC) using an amplifier (OC-725; Warner Instruments, Hamden, CT). Acquired data were digitized using an AD/DA converter Digidata 1440 A running under pClamp at room temperature (22–24 °C). Output signals were digitized at 10 kHz. The bath solution was ND96, the glass electrodes were filled with 3 M KCl, and the resistances ranged from 0.2–1.0 MΩ. The holding potential was −60 mV.

Antibodies

Commercially obtained antibodies include goat polyclonal anti-BASIGIN (sc-9757, Santa Cruz, Santa Cruz, CA, USA), mouse monoclonal anti-β-Tubulin IV (T7941, Sigma-Aldrich), anti-HA (MMS-101R, Covance, Berkeley, CA, USA), Alexa Fluor 488-conjugated chicken anti-rat IgG (A-21470, Invitrogen, Carlsbad, CA, USA), Alexa Fluor 594-conjugated goat anti-mouse IgG (A-11005, Invitrogen), HRP-linked anti-rabbit or mouse secondary antibodies (NA9340V or NA9310V; GE Healthcare, Pittsburgh, PA, USA), and HRP-linked anti-goat secondary antibody (sc-2354; Santa Cruz Biotechnology). The VSP antibody used was the same as in our previous study[8]. The rat monoclonal anti-IZUMO1 antibody was generated previously[47].

Isolation of Different Stages of Spermatids and Spermatozoa for PIPs Measurement

Mature and immature spermatozoa were isolated from cauda and caput epididymis, respectively. After making an incision in the epididymis, the tissues were stirred in an HS-based solution. After counting the cells, the sperm were centrifuged at 500 *g* for 5 min at 4 °C. The pellets were washed with PBS and centrifuged again at 500 *g* for 5 min at 4 °C. The pellets were then frozen and used for analysis.

For isolation of testicular spermatozoa and spermatids, we modified a previously reported two-step enzymatic digestion method[48]. Seminiferous tubules were dissociated with collagenase type I (1.0 mg/mL; Sigma-Aldrich) for 25 min at 32 °C in incubation medium; Hanks' balanced salt solution (HBSS) supplemented with 20 mM HEPES (pH 7.2), 1.2 mM $MgSO_4$, 1.3 mM $CaCl_2$, 6.6 mM sodium pyruvate, and 0.05% lactate. Tubules were collected, and after a filtration step with a 40-μm nylon mesh, tubules were retained in the filter. The tubules were collected again and incubated at 32 °C for 25 min in the same collagenase buffer. The resulting whole cell suspension was filtered through a 40-μm nylon mesh to remove cell clumps. For testicular spermatozoa, the suspension was centrifuged at 300 *g* for 5 min at 4 °C and supernatant was collected. The sediment was used for spermatids collection as described later. The supernatant fraction was centrifuged with 800 *g* for 5 min at 4 °C, and then the supernatant was removed. After adding 1 mL incubation medium, it was centrifuged again at 800 *g* for 5 min at 4 °C. The pellet contained high purity of testicular spermatozoa (Supplementary Fig. 5b). For isolation of spermatids, we used the above-mentioned sediment for flow cytometry and cell sorting as previously reported[48,49]. The cells were stained with Hoechst 33258 (5 μg/million cells; Dojindo, Kumamoto, Japan) for more than 30 min at room temperature. BD FACSAria IIIu was used for flow cytometry and cell sorting. Hoechst was excited using a 375 nm laser, and the dye's wide emission spectrum detected in two distinct channels: "Hoechst Blue" (450/20 nm band-pass filter) and "Hoechst Red" (670 nm long pass filter). Forward Scatter (FSC-A) and Side Scatter (SSC-A) were detected using a 488 nm laser. The fraction of spermatids was collected in incubation medium (Supplementary Fig. 5a) and centrifuged at 8000 *g* for 5 min at 4 °C. The cells were obtained from the pellet.

PIPs sample preparation

Mass spectrometric analyses of PIPs was performed as previously reported[19]. Frozen sperm samples were thawed and suspended in 1.5 mL of methanol. To this suspension, 50 μL of a methanol/chloroform (9/1) solution containing 1 nmol of C8:0/C8:0 $PI(4,5)P_2$ (serving as an absorption inhibitor) and 10 pmol each of synthetic C17:0/C20:4 phosphoinositide as internal standards were added. This mixture was then combined with 750 μL of ultrapure water, 750 μL of 2 M HCl, and 200 μL of 1 M NaCl. Following a thorough vortex-mixing, 3 mL of chloroform was added, and the mixture was vortexed again for 2 min. The resulting solution was centrifuged at 1200 g for 4 min at room temperature. The lower organic phase, which contains the crude lipid extract, was carefully collected and transferred into a fresh glass tube. PIPs were preconcentrated using an anion exchanging resin. DEAE Sepharose Fast Flow (10% slurry) was sequentially rinsed: twice with an equal volume of ultrapure water, once with 1 M HCl, twice again with

ultrapure water, once with 1 M NaOH, and then twice with ultrapure water. The resin was then resuspended in methanol to create a 50% slurry, and a 0.5 mL bed volume was packed into a Pasteur pipette plugged with glass wool. The crude lipid extract (2.9 mL) was mixed with 1.5 mL methanol and applied to the column. The column was washed with 3 mL of a chloroform/methanol (1/1) solution, followed by 2 mL of a chloroform/methanol/28% aqueous ammonia/glacial acetic acid (200/100/3/0.9) solution. Elution was performed using 1.5 mL of chloroform/methanol/12 M hydrochloric acid/ultrapure water (12/12/1/1). The eluate was then mixed with 850 μL of 120 mM NaCl and centrifuged at 1200 g for 4 min at room temperature. The lower phase, containing purified PIPs, was collected into a fresh glass tube. The purified PIPs were derivatized through methylation, following the method of Clark et al[50]. Briefly, 150 μL of 0.6 M trimethylsilyl diazomethane was added to the purified phosphoinositide fraction prepared as described above at room temperature. After 10 min, the reaction was stopped by adding 20 μL of glacial acetic acid. The samples were then mixed with 700 μL of a methanol/ultrapure water/chloroform (48/47/3) solution, followed by 1 minute of vortexing. After centrifugation at 1200 g for 4 min, the lower phase was dried under a stream of nitrogen and redissolved in 100 μL of acetonitrile.

PI4P/PI(4,5)P_2 measurements by PRMC-MS

Phosphoinositide regioisomer measurement by chiral column chromatography and mass stepctrometery (PRMC-MS) was conducted using a QTRAP6500 triple quadrupole mass spectrometer (ABSciex) paired with a Nexera X2 HPLC system (Shimadzu) and a PAL HTC-xt (CTC Analytics) autosampler. Spectra were recorded in positive ion mode as $[M + NH_4]^+$ ions, with an MS/MS scan duration of 0.5 sec. The ion spray voltage was set to 5.5 kV, cone voltage to 30 V, and source block temperature to 100 °C. The curtain gas was set to 20 psi, collision gas to 9 psi, ion source gas pressures 1/2 to 50 psi, declustering potential to 100 V, entrance potential to 10 V, and collision cell exit potential to 12 V. Collision energy values for gas phase fragmentation are detailed in Supplementary Table 2. A 10 μL lipid sample was injected using the autosampler, and lipids were separated using a CHIRALPAK IC-3 column (2.1 mmφ x 250 mm, 3 μm, DAICEL) in a 22 °C room. The liquid column chromatography was conducted at a flow rate of 100 μL/min with the following gradient: 40% mobile phase A (methanol/5 mM ammonium acetate) and 60% mobile phase B (acetonitrile/5 mM ammonium acetate) held for 1 minute, linearly increased to 85% mobile phase A over 2 min and maintained at 85% mobile phase A for 11 min. Data acquisition and processing were performed using Analyst 1.6.3 (SCIEX), while MultiQuant (SCIEX) was used for manual data evaluation and peak integration. No background subtraction was carried out, and Gaussian smoothing width was set to 1.0 points. For quality control, peaks from samples where the cps of the surrogate internal standards (SIS; C37:4 PIPs) from the multiple reaction monitoring (MRM) scan were below 2×10^4 were excluded from quantification analysis. The sample peak area value was divided by the corresponding SIS peak area value (equivalent to 1 pmol) to achieve relative quantification. Supplementary Table 3 lists the MRM transitions (pairs of m/z values of precursor ions and fragment/diacylglycerol ions) used for the identification and quantification of each PI4P/PI(4,5)P_2 molecular species.

Reverse phase (RP) LC-MS/MS analysis

An Ultimate 3000 LC system (Thermo Fisher Scientific) was used for the RP LC-MS/MS analysis, connected in tandem to a TSQ Vantage triple stage quadrupole mass spectrometer (Thermo Fisher Scientific) operating in positive-ion mode. The derivatized phospholipids (the injection volume was 20 μL, and the flow rate was set at 220 μL/min) were separated on an InertSustainBio C18 column (GL Sciences) with the following solvent gradient: 0–1 minute hold at 70% A/30% B, 1–3 min linear gradient to 90% A/10% B, 3–7.5 min constant at 90% A/10% B, and 7.5–13 min at 30% A/70% B. Here, mobile phase A consisted of acetonitrile/ ultrapure water/70% ethylamine (800:200:1.3), and mobile phase B consisted of isopropanol/acetonitrile/70% ethylamine (800:200:1.3). Measurement of PIP and PIP_2 species was achieved through MRM using a pre-set list of mass to charge ratio values (Supplementary Table 4). Spray voltage was set to 3250 V, sheath gas pressure to 15 arbitrary units, capillary temperature to 300 °C. Supplementary Table 5 lists the voltage for fragmentation. Data acquisition and processing and peak integration were performed using Xcalibur software 2.0 (Thermo Fisher Scientific). The quantification was achieved by dividing the sample peak area value by the corresponding the internal standard peak area value.

Western blotting from spermatozoa

Sperm were isolated from caput and cauda epididymis. They were rotated at 4 °C for 1 hour in a lysis solution containing: 10 mM Tris-HCl (pH 7.5), 50 mM KCl, 1% Triton X-100, and cOmplete™ Protease Inhibitor Cocktail (Roche). After centrifugation (9000 g for 5 min at 4 °C), the supernatant was mixed with sample buffer and 2.5% 2-ME. After SDS-PAGE, the proteins were transferred to a PVDF membrane. After blocking with 0.5% skim milk or 2% BSA, the blots were incubated with the primary antibody: anti-VSP (1:500) or anti-BASIGIN (1:500) in Can get signal 1 (Toyobo, Osaka, Japan). The membranes were washed and incubated with HRP-linked anti-rabbit or goat antibody (1:1000) in Can get signal 2 (TOYOBO). The signals were detected with ECL Prime Western Blotting Detection Reagent (GE Healthcare). Images were acquired using a CS analyzer system (ver. 3) (ATTO, Tokyo, Japan). Antibody stripping was sometimes performed using 200 mM Glycine (pH 2.8) for 10 min at 60 °C for other antibody experiments. The signal intensity of individual bands was calculated by subtracting the background intensity.

Western blotting of membrane proteins from Xenopus oocytes

Two days prior to the experiment, *Xenopus* oocytes were injected with cRNA. They were then placed in ND96 solution containing EZ-Link Sulfo-NHS-SS-Biotin (0.5 mg/mL, Thermo Fisher Scientific) for 30 min at room temperature. Cells were washed with PBS three times and quenched with lysed in 300 μL PBS supplemented with Triton X-100 (1%; Sigma Aldrich) and Complete protease inhibitor cocktail tablets without EDTA (Roche, Basel, Switzerland). After centrifugation (15310 *g* for 10 min at 4 °C), 150 μL of the supernatant was retained as "total lysate," and the rest was incubated overnight at 4 °C under gentle rotation with 30 μL streptavidin agarose beads (COSMO BIO, Tokyo, Japan) pre-washed with PBS. The beads were collected by centrifugation (15310 *g* for 10 min at 4 °C) and washed with PBS containing 1% Triton X-100 three times. Biotinylated proteins were eluted from the streptavidin agarose beads by incubating in SDS-PAGE sample buffer containing 2.5% 2-ME for 30 min at room temperature ("Cell surface"). Total lysates were also mixed with SDS-PAGE sample buffer with 2.5% 2-ME. After SDS-PAGE for the supernatant, the proteins were transferred to a PVDF membrane. After blocking with 0.5% skim milk the blots were incubated with the primary antibody: anti-HA (1:2000, Covance, Berkeley, CA) in Can get signal 1 (Toyobo, Osaka, Japan). The membranes were washed and incubated with HRP-linked anti-mouse antibody (1:2000, Cytiva, Massachusetts, USA) in Can get signal 2 (TOYOBO). The signals were detected with ECL Prime Western Blotting Detection Reagent (GE Healthcare). Images were acquired using a CS analyzer system (ver. 3) (ATTO, Tokyo, Japan).

Sperm motility analysis

Sperm velocity was analyzed as described previously[51]. Spermatozoa isolated from the cauda epididymis were suspended in TYH medium, a well-established capacitation-inducing medium[52]. TYH contains: 120 mM NaCl, 4.8 mM KCl, 1.2 mM KH_2PO_4, 5.6 mM glucose, 1.0 mM sodium pyruvate, 1.7 mM $CaCl_2$, 1.2 mM $MgSO_4$, 25 mM $NaHCO_3$, 4.0 g/L ALBMAX I (Thermo Fisher Scientific), penicillin (50 units/mL)-

streptomycin (50 µg/mL), and 0.6% Phenol-red. Average path velocity (VAP), curvilinear velocity (VCL), straight-line velocity (VSL), and Amplitude of Lateral Head Displacement (ALH) were measured using the CEROS II sperm analysis system (Hamilton Thorne Biosciences, MA, USA) at 10 min and 2 h after incubation. Sperm motility was videotaped with an Olympus BX-53 microscope equipped with a high-speed camera (HAS-L1, Ditect, Tokyo, Japan) at 200 frames per second. The trajectory was visualized with 450 frames using ImageJ software (NIH) and plug-in Color Footprint Rainbow developed by Y. Hiratsuka (JAIST, Ishikawa, Japan).

Voltage Clamp Fluorometry (VCF) recording with PHPLCδ1-GFP

The plasmid of the GFP-fused pleckstrin homology domain from the PLCδ1 subunit (PHPLCδ1-GFP) was used as previously reported[53]. The microscope BX50WI upright fluorescence microscope (Olympus, Japan) was used with a 20 × 0.75 N.A. objective lens and LED lamp (MCWHL8: Thorlabs, Inc., New Jersey, USA), fitted with an excitation filter of BP460-480HQ (Olympus) and an emission filter of BA495-540HQ (Olympus). The emitted light is detected by a PMT (H10722-20; Hamamatsu Photonics, Japan). TEVC recording was done using the amplifier, Oocyte Clamp OC-725C (Warner Instruments, USA). Data were digitized using Digidata 1440A (Molecular Devices, USA) run by the software pClamp 10.3 (Molecular Devices, USA) with a 10 kHz sampling rate on Windows PC. After digitization, data were digitally filtered at a cut-off frequency of 50 Hz on pClamp. The bath solution was ND96, and the glass electrodes were filled with 3 M K^+-acetate and 10 mM KCl. The resistances ranged from 0.2-1.0 MΩ. The holding potential was −80 mV. A depolarizing pulse (−50 to 125 mV) was applied for 10 s.

Generation of VSP point-mutation knock-in mice

In this study, we generated D225R, V312R, and K347Q mice. C57BL/6 fertilized eggs were obtained by in vitro fertilization. Oligonucleotides (200 ng/µl) and crRNA/tracrRNA/Cas9 ribonucleoproteins (40 ng/µl crRNA plus tracrRNA, 100 ng/µl CAS9) were electroporated into the fertilized eggs using a super electroporator NEPA21 (NEPA GENE, Chiba, Japan) (poring pulse, voltage: 225 V, pulse width: 2 ms, pulse interval: 50 ms, and number of pulses: +4; transfer pulse, voltage: 20 V, pulse width: 50 ms, pulse interval: 50 ms, and number of pulses: ±5). The reference oligonucleotides contained the point mutations D225R, V312R, and K347Q, respectively. Furthermore, it contains silent mutations that prevent recutting of the target sequences and allow recognition by the restriction enzyme for convenient genotyping (Fig. 4 and Supplementary Fig. 6). The reference oligonucleotides are listed in Supplementary Table 6. One out of 25, 8 out of 24, and 5 out of 15 pups contained the expected mutations in D225R, V312R, and K347Q, respectively. The animals were crossed with C57BL/6 mice to expand the colony. The genotype primers for each knock-in mouse are as follows: D225R, 5′−GGGGCTTGGTGCATACTTTA−3′ and 5′−AGC TGTGACAAAGCCACTG−3′; V312R, 5′−CATTGCCCTTTGTCTTCTAC−3′ and 5′−ATTGGGAAATCATAAAGCTG−3′; K347Q, 5′−CCTTGTGTCT CGGGGAAATA−3′ and 5′−GCTCACGTGACTCAGGGAAT−3′.

Immunocytochemistry for isolated spermatid and testicular spermatozoa

The isolated spermatids or spermatozoa in incubating medium were seeded on 1 mg/mL poly-L-lysine coated coverslips. After 1 h, the sample was fixed with 4% PFA/PBS. Cells were washed with 0.3% PBST. For the primary antibody, a rat monoclonal anti-IZUMO1 (1:500 dilution) and anti-β-Tubulin IV (1:500 dilution) was used with 10 % goat serum. The binding of the primary antibody was detected using Alexa Fluor 488-conjugated chicken anti-rat IgG (1:2000 dilution) and Alexa Fluor 594-conjugated goat anti-moue IgG (1:2000 dilution). Confocal images were acquired using a LSM770 confocal laser scanning system (Carl Zeiss, Germany).

Litter size analysis

Male mice of each genotype were crossed with 8 − 11 weeks old of wild-type female mice. The number of pups was defined as litter size.

In vitro fertilization

Mature cumulus intact oocytes were collected from wildtype females and placed in a drop of 100 µl TYH medium. Spermatozoa were collected from cauda epididymis of male mouse and incubated in TYH medium for 2 h to induce capacitation. Capacitated spermatozoa were added to the TYH drop containing oocytes at a final concentration of $2 \times 10^{\wedge 5}$ sperm/ml. Embryos reaching the two-cell stage by the next day were counted as fertilized.

Data Analysis

Data analysis was performed with Excel 2016 (Microsoft, USA), Clampfit 10.5 (Molecular Device, USA), and Igor Pro 6.37 (WaveMetrics, USA) software. Statistical analysis was performed with Prism 6 (GraphPad Software, San Diego, CA). For two-group comparison, we conducted an unpaired t-test or Mann-Whitney test as appropriate. An outlier was detected with Grubbs' Test (α = 0.05) in individual experiment groups and removed from the analysis (Fig. 5c, d). For multiple comparisons, we conducted multiple *t*-test, Dunnett's multiple comparisons or Tukey's test as appropriate. Data are represented as mean ± s.e.m. *, **, ***, and **** indicate a significant difference: $p < 0.05$, $p < 0.01$, $p < 0.001$, and $p < 0.0001$, respectively.

Reporting summary

Further information on research design is available in the Nature Portfolio Reporting Summary linked to this article.

Data availability

The data generated in this study are provided in the main text or the Supplemental materials. Source data are provided with this paper.

References

1. Hille B. *Ion channels of excitable membranes*. Sinauer Associates Inc, Sunderland (2001).
2. Murata, Y., Iwasaki, H., Sasaki, M., Inaba, K. & Okamura, Y. Phosphoinositide phosphatase activity coupled to an intrinsic voltage sensor. *Nature* **435**, 1239–1243 (2005).
3. Okamura, Y., Kawanabe, A. & Kawai, T. Voltage-sensing phosphatases: biophysics, physiology, and molecular engineering. *Physiol. Rev.* **98**, 2097–2131 (2018).
4. Okamura, Y. Biodiversity of voltage sensor domain proteins. *Pflug. Arch.: Eur. J. Physiol.* **454**, 361–371 (2007).
5. Okamura, Y. & Dixon, J. E. Voltage-sensing phosphatase: its molecular relationship with PTEN. *Physiology* **26**, 6–13 (2011).
6. Okamura, Y., Fujiwara, Y. & Sakata, S. Gating mechanisms of voltage-gated proton channels. *Annu. Rev. Biochem.* **84**, 685–709 (2015).
7. Okamura, Y., Murata, Y. & Iwasaki, H. Voltage-sensing phosphatase: actions and potentials. *J. Physiol.* **587**, 513–520 (2009).
8. Kawai, T. et al. Polarized PtdIns(4,5)P(2) distribution mediated by a voltage-sensing phosphatase (VSP) regulates sperm motility. *Proc. Natl Acad. Sci. USA* **116**, 26020–26028 (2019).
9. Zeng, X. H., Yang, C., Kim, S. T., Lingle, C. J. & Xia, X. M. Deletion of the Slo3 gene abolishes alkalization-activated K+ current in mouse spermatozoa. *Proc. Natl Acad. Sci. USA* **108**, 5879–5884 (2011).
10. Santi, C. M. et al. The SLO3 sperm-specific potassium channel plays a vital role in male fertility. *FEBS Lett.* **584**, 1041–1046 (2010).
11. Hossain, M. I. et al. Enzyme domain affects the movement of the voltage sensor in Ascidian and Zebrafish voltage-sensing phosphatases. *J. Biol. Chem.* **283**, 18248–18259 (2008).

12. Kurokawa, T. et al. 3′ Phosphatase activity toward phosphatidylinositol 3,4-bisphosphate [PI(3,4)P_2] by voltage-sensing phosphatase (VSP). *Proc. Natl Acad. Sci. USA* **109**, 10089–10094 (2012).
13. Yamaguchi, S. et al. Potential role of voltage-sensing phosphatases in regulation of cell structure through the production of PI(3,4)P_2. *J. Cell. Physiol.* **229**, 422–433 (2014).
14. Ratzan, W. J., Evsikov, A. V., Okamura, Y. & Jaffe, L. A. Voltage sensitive phosphoinositide phosphatases of Xenopus: their tissue distribution and voltage dependence. *J. Cell. Physiol.* **226**, 2740–2746 (2011).
15. Rosasco, M. G., Gordon, S. E. & Bajjalieh, S. M. Characterization of the functional domains of a mammalian voltage-sensitive phosphatase. *Biophys. J.* **109**, 2480–2491 (2015).
16. Nikolopoulou, M., Soucek, D. A. & Vary, J. C. Changes in the lipid content of boar sperm plasma membranes during epididymal maturation. *Biochim. et. Biophys. Acta* **815**, 486–498 (1985).
17. Rooke, J. A., Shao, C. C. & Speake, B. K. Effects of feeding tuna oil on the lipid composition of pig spermatozoa and in vitro characteristics of semen. *Reproduction* **121**, 315–322 (2001).
18. Lin, D. S., Connor, W. E., Wolf, D. P., Neuringer, M. & Hachey, D. L. Unique lipids of primate spermatozoa: desmosterol and docosahexaenoic acid. *J. lipid Res.* **34**, 491–499 (1993).
19. Morioka, S. et al. A mass spectrometric method for in-depth profiling of phosphoinositide regioisomers and their disease-associated regulation. *Nat. Commun.* **13**, 83 (2022).
20. Wu, Y. et al. PTEN 2, a Golgi-associated testis-specific homologue of the PTEN tumor suppressor lipid phosphatase. *J. Biol. Chem.* **276**, 21745–21753 (2001).
21. Arima, H., Tsutsui, H. & Okamura, Y. Conservation of the Ca(2+)-permeability through the voltage sensor domain of mammalian CatSper subunit. *Channels* **12**, 240–248 (2018).
22. Kawanabe, A. et al. Engineering an enhanced voltage-sensing phosphatase. *J. Gen. Physiol.* **152**, e201912491 (2020).
23. Langlhofer, G. & Villmann, C. The intracellular loop of the glycine receptor: it's not all about the size. *Front. Mol. Neurosci.* **9**, 41 (2016).
24. Nasu-Nishimura, Y. et al. Identification of an endoplasmic reticulum-retention motif in an intracellular loop of the kainate receptor subunit KA2. *J. Neurosci.* **26**, 7014–7021 (2006).
25. Marku, A. et al. The LRRK2 N-terminal domain influences vesicle trafficking: impact of the E193K variant. *Sci. Rep.* **10**, 3799 (2020).
26. Li, Q. et al. Structural mechanism of voltage-dependent gating in an isolated voltage-sensing domain. *Nat. Struct. Mol. Biol.* **21**, 244–252 (2014).
27. Tsutsui, H., Higashijima, S., Miyawaki, A. & Okamura, Y. Visualizing voltage dynamics in zebrafish heart. *J. Physiol.* **588**, 2017–2021 (2010).
28. Tsutsui, H., Jinno, Y., Tomita, A. & Okamura, Y. Rapid evaluation of a protein-based voltage probe using a field-induced membrane potential change. *Biochim. et. Biophysica Acta* **1838**, 1730–1737 (2014).
29. Dimitrov, D. et al. Engineering and characterization of an enhanced fluorescent protein voltage sensor. *PLoS One* **2**, e440 (2007).
30. Kohout, S. C., Ulbrich, M. H., Bell, S. C. & Isacoff, E. Y. Subunit organization and functional transitions in Ci-VSP. *Nat. Struct. Mol. Biol.* **15**, 106–108 (2008).
31. Villalba-Galea, C. A., Sandtner, W., Starace, D. M. & Bezanilla, F. S4-based voltage sensors have three major conformations. *Proc. Natl Acad. Sci. USA* **105**, 17600–17607 (2008).
32. Villalba-Galea, C. A. Voltage-controlled enzymes: the new Janus-Bifrons. *Front. Pharmacol.* **3**, 161 (2012).
33. Mutua, J. et al. Functional diversity of voltage-sensing phosphatases in two urodele amphibians. *Physiol. Rep.* **2**, e12061 (2014).
34. Kohout, S. C. et al. Electrochemical coupling in the voltage-dependent phosphatase Ci-VSP. *Nat. Chem. Biol.* **6**, 369–375 (2010).
35. Rejraji, H. et al. Lipid remodeling of murine epididymosomes and spermatozoa during epididymal maturation. *Biol. Reprod.* **74**, 1104–1113 (2006).
36. Hasegawa, H. et al. Phosphatidylinositol 4-phosphate 5-kinase is indispensable for mouse spermatogenesis. *Biol. Reprod.* **86**, 131–112 (2012).
37. Paixao, I. C. et al. Role of K364 next to the active site cysteine in voltage-dependent phosphatase activity of Ci-VSP. *Biophys. J.* **122**, 2267–2284 (2023).
38. Shen, R., Meng, Y., Roux, B. & Perozo, E. Mechanism of voltage gating in the voltage-sensing phosphatase Ci-VSP. *Proc. Natl Acad. Sci. USA* **119**, e2206649119 (2022).
39. Levine, N. & Marsh, D. J. Micropuncture studies of the electrochemical aspects of fluid and electrolyte transport in individual seminiferous tubules, the epididymis and the vas deferens in rats. *J. Physiol.* **213**, 557–570 (1971).
40. Jenkins, A. D., Lechene, C. P. & Howards, S. S. Concentrations of seven elements in the intraluminal fluids of the rat seminiferous tubules, rate testis, and epididymis. *Biol. Reprod.* **23**, 981–987 (1980).
41. Scott, T. W., Wales, R. G., Wallace, J. C. & White, I. G. Composition of Ram epididymal and testicular fluid and the biosynthesis of glycerylphosphorylcholine by the rabbit epididymis. *J. Reprod. Fertil.* **6**, 49–59 (1963).
42. Verberckmoes, S., Van Soom, A., Dewulf, J., De Pauw, I. & de Kruif, A. Storage of fresh bovine semen in a diluent based on the ionic composition of cauda epididymal plasma. *Reprod. Domest. Anim.* **39**, 410–416 (2004).
43. Cong, L. et al. Multiplex genome engineering using CRISPR/Cas systems. *Science* **339**, 819–823 (2013).
44. Mashiko, D. et al. Generation of mutant mice by pronuclear injection of circular plasmid expressing Cas9 and single-guided RNA. *Sci. Rep.* **3**, 3355 (2013).
45. Inanobe, A. et al. Molecular cloning and characterization of a novel splicing variant of the Kir3.2 subunit predominantly expressed in mouse testis. *J. Physiol.* **1**, 19–30 (1999).
46. Kirichok, Y., Navarro, B. & Clapham, D. E. Whole-cell patch-clamp measurements of spermatozoa reveal an alkaline-activated Ca2+ channel. *Nature* **439**, 737–740 (2006).
47. Ikawa, M. et al. Calsperin is a testis-specific chaperone required for sperm fertility. *J. Biol. Chem.* **286**, 5639–5646 (2011).
48. Bastos, H. et al. Flow cytometric characterization of viable meiotic and postmeiotic cells by Hoechst 33342 in mouse spermatogenesis. *Cytom. A* **65**, 40–49 (2005).
49. Gaysinskaya, V. & Bortvin, A. Flow cytometry of murine spermatocytes. *Curr. Protoc. Cytom.* **72**, 44 41–47 44 24 (2015).
50. Clark, J. D. et al. A novel arachidonic acid-selective cytosolic PLA_2 contains a Ca^{2+}-dependent translocation domain with homology to PKC and GAP. *Cell* **65**, 1043–1051 (1991).
51. Miyata, H. et al. SPATA33 localizes calcineurin to the mitochondria and regulates sperm motility in mice. *Proc. Natl Acad Sci. USA* **118**, e2106673118 (2021).
52. Toyoda, T., Yokoyama, M. & Hosi, T. Studies on the fertilization of mouse eggs in vitro. I. In vitro fertilization of eggs by fresh epididymal sperm. *Jpn J. Anim. Reprod.* **16**, 147–151 (1971).
53. Murata, Y. & Okamura, Y. Depolarization activates the phosphoinositide phosphatase Ci-VSP, as detected in Xenopus oocytes coexpressing sensors of PIP_2. *J. Physiol.* **583**, 875–889 (2007).
54. Mirdita, M. et al. ColabFold: making protein folding accessible to all. *Nat. Methods* **19**, 679–682 (2022).

Acknowledgements

We express our gratitude to Ms. Hikari Ginama, Ms. Megumi Kobayashi, and Dr. Natsuki Mizutani from Osaka University, Dr. Hiroki Nakanishi from Akita University, and NPO Biotechnology Research and Development for

their technical support. We also thank Ms. Risa Mori-Kreiner for critical reading of the manuscript. This study received support from the Center for Medical Research and Education at the Graduate School of Medicine, Osaka University, and JSPS KAKENHI Grant Number JP20KK0376 (AdAMS) to T.K. Funding was provided by Grants-in-Aid from JSPS KAKENHI Grant Numbers JP17K15558, JP20K07274, JP20KK0376, JP23K06334 and JST FOREST Program, Grant Number JPMJFR225Z. Additionally, financial support was received from The Ichiro Kanehara Foundation, the Hyogo Science and Technology Association, the Sumitomo Foundation, the Ono Medical Research Foundation, the Uehara Memorial Foundation, the Senri Life Science Foundation, the Takeda Science Foundation, and Mochida Memorial Foundation for Medical and Pharmaceutical Research, all of which contributed to T.K.'s research. T.S. was supported by AMED under Grant Number 24gm1710007, by TMDU under Multilayered Stress Diseases (JPMXP1323015483), and Medical Research Center Initiative for High Depth Omics. This work was also supported by MEXT KAKENHI Grant Numbers JP15H05901, JP20H05791) and JSPS KAKENHI Grant Numbers JP21229003, JP25253016, JP19H03401 to Y.Okamura.

Author contributions

T.K. and Y.Okamura conceived the study; T.K. and Y.Okamura designed experiments; T.K., H.M, Y.Oyama, and R.I.N performed and M.I. supervised experiments for in vitro fertilization and sperm motility analysis; T.K, S.A. and G.T performed FACS for spermatids isolation; S.M. performed experiments for LC/MS-MS analysis and J.S and T.S supervised them; T.N and H.M generated knock-in mice and knock-out mice; K. S provided VSP-deficient mice; M.W provided the antibody for VSP; T.K and R.T.A performed VCF experiments; T.K performed experiments for immunocytochemistry, Western blotting, and electrophysiology. T.K. drafted the manuscript; All members critically read the manuscript.

Competing interests

The authors declare no competing interests.

Additional information

Supplementary information The online version contains supplementary material available at https://doi.org/10.1038/s41467-024-51755-2.

Correspondence and requests for materials should be addressed to Takafumi Kawai.

Peer review information *Nature Communications* thanks Laurinda Jaffe, Michael Nomikos and Elisabeth Pinart for their contribution to the peer review of this work. A peer review file is available.